Review Paper
J. Astron. Space Sci. 39(2), 23-33 (2022)
https://doi.org/10.5140/JASS.2022.39.2.23

JASS Journal of Astronomy and Space Sciences

The Occurrence Climatology of Equatorial Plasma Bubbles: A Review

Hyosub Kil†
The Johns Hopkins University Applied Physics Laboratory, Laurel, MD 20723, USA

Electron density irregularities in the equatorial ionosphere at night are understood in terms of plasma bubbles, which are produced by the transport of low-density plasma from the bottomside of the F region to the topside. Equatorial plasma bubbles (EPBs) have been detected by various techniques on the ground and from space. One of the distinguishing characteristics of EPBs identified from long-term observations is the systematic seasonal and longitudinal variation of the EPB activity. Several hypotheses have been developed to explain the systematic EPB behavior, and now we have good knowledge about the key factors that determine the behavior. However, gaps in our understanding of the EPB climatology still remain primarily because we do not yet have the capability to observe seed perturbations and their growth simultaneously and globally. This paper reviews the occurrence climatology of EPBs identified from observations and the current understanding of its driving mechanisms.

Keywords: equatorial ionosphere, plasma bubble, irregularities

1. INTRODUCTION

Severe ionospheric turbulences occur at night in the equatorial F region through the phenomenon known as "plasma bubbles." Plasma bubbles are produced by the transport of low-density plasma from the bottomside of the F region to the topside, where the plasma density is higher. As a result, plasma bubbles appear as plasma depletions with respect to ambient plasma in the topside. The generation mechanism of a bubble and its three-dimensional structure are discussed in the review by Kil (2015) and references therein. Equatorial plasma bubbles (EPBs) have been observed for about a century by using various techniques on the ground and from space. A distinguishing behavior of EPBs identified from a range of observations is that EPB activity systematically varies with season and longitude. The data also show a dependence on the solar cycle. These three factors (season, longitude, and solar cycle) provide a basic framework with which to understand the climatological behavior of EPBs.

This review focuses on the climatological behavior of EPBs and its drivers. Occasionally, deviations from the usual climatological behavior are caused by known natural phenomena, such as geomagnetic activity, volcanoes, earthquakes, and tropical storms. The EPB climatology is not affected by these deviations because the aggregate anomalous days make up only a small portion of the total observation days. Because the physical processes underlying the EPB climatology are generally applicable to any conditions, the deviations can also be explained on the basis of the driving mechanisms of the climatology.

The sample measurement of plasma density in Fig. 1 shows the development of different types of irregularities in the low-latitude F region (Kil et al. 2020). The observation was made by the first Republic of China satellite (ROCSAT-1) at an altitude of 600 km on 19 August 2003. The red shading indicates typical nighttime EPBs. The plasma density for some of the EPBs is more than an order of magnitude lower than the background. Small amplitude irregularities (yellow shading) also develop at night, but their morphology is different from the EPB morphology in red shading. The different characteristics of the irregularities can be

Received 17 APR 2022 **Revised** 17 MAY 2022 **Accepted** 05 JUN 2022
†**Corresponding Author**
Tel: +1-240-228-6353, E-mail: Hyosub.kil@jhuapl.edu
ORCID: https://orcid.org/0000-0001-8288-6236

http://janss.kr pISSN: 2093-5587 eISSN: 2093-1409

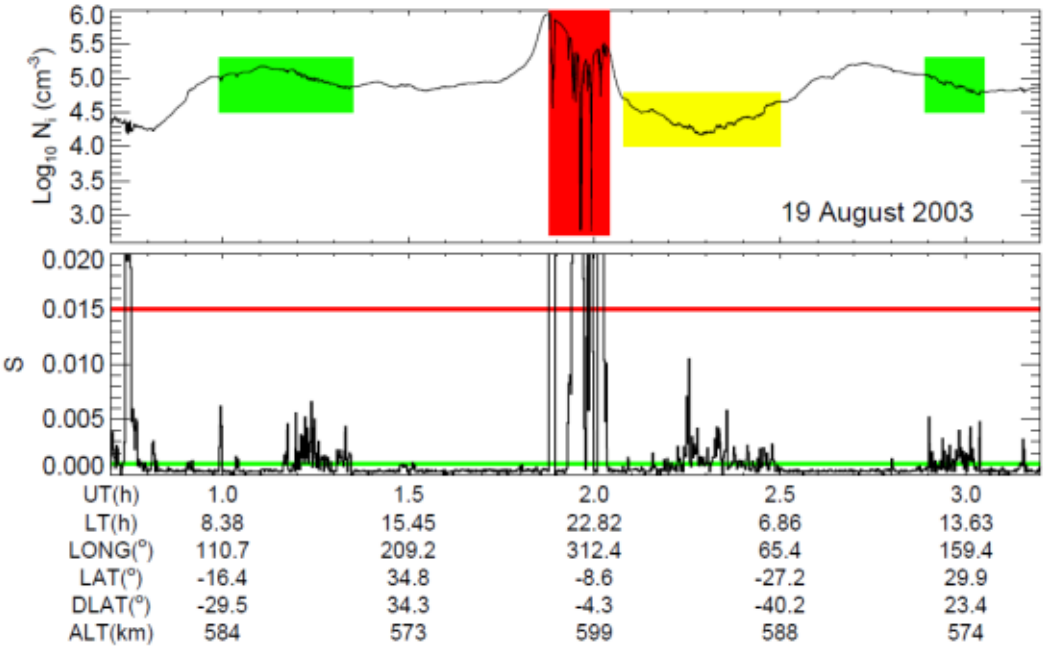

Fig. 1. Different types of irregularities in the topside. Adapted from Kil et al. (2020) with CC-BY. (Top) Electron density irregularities detected by ROCSAT-1 on 19 August 2003. Red shading indicates typical premidnight EPBs. Small-amplitude irregularities at night and on the dayside are indicated with yellow and green shading. (Bottom) Irregularity index S. In previous studies, nighttime EPBs were detected by using the threshold around S = 0.015. S = 0.001 (green line) can be used as a threshold for the detection of small-amplitude irregularities. ROCSAT-1, Republic of China satellite; EPB, equatorial plasma bubble.

related to differences in the detection time, latitude, or generation mechanism. The green shaded areas indicate the irregularities detected on the dayside. The bottom plot is the irregularity index S defined as

$$S=\left[\frac{1}{n-1}\sum_{i=0}^{n-1}\left(\log_{10}N_i-L_i\right)^2\right]^{1/2} \quad (1)$$

Here N_i is the electron density, L_i is the linear fit of $\log_{10} N_i$, and n is the number of data points. S was calculated for n = 10 (10-second data).

Because large-amplitude EPBs are of primary interest, many studies used a threshold similar to the one indicated by the red line (S = 0.015) for the EPB detection. The currently established EPB climatology is primarily based on intense EPBs, such as those indicated by red shading. The baseline of the S value is ~0.0005. The small-amplitude irregularities above this baseline can be detected by using the threshold 0.001 (green line). Daytime irregularities in Section 4 are detected by using this threshold. The small amplitude irregularities at night (yellow shading) are also interesting phenomena, but this review does not address these irregularities because we do not yet know enough about their behavior and origin to establish their climatology.

2. CLIMATOLOGY OF NIGHTTIME EQUATORIAL PLASMA BUBBLEs (EPBs)

The observation of radio scintillations at stations in proximity to the magnetic equator revealed different seasonal behavior at different longitudes (Basu & Basu 1981; Aarons 1982, 1993; Tsunoda 1985 and references therein). In South America, for example, strong scintillations occurred frequently around December solstices, whereas they rarely occurred around June solstices. The opposite annual behavior was observed in the Asian sector. The electron density irregularities in the topside ionosphere also showed similar seasonal behavior (Hanson & Sanatani 1971; Basu et al. 1976; Burke et al. 1979). Because EPBs are the primary source of scintillations and electron density irregularities in the equatorial region, these observations illustrate the seasonal and longitudinal behavior of EPBs.

The ground-based scintillation observations and early satellite detection of irregularities provided only partial information about EPB behavior because scintillation observations were not available over the ocean and satellite observations were only made for limited periods. The global morphology of irregularities (or EPBs) and their seasonal variation were first derived from a topside sounding experiment by the Ionosphere Sounding Satellite b (ISS-b) (Maruyama & Matuura 1984). ISS-b had a nearly circular

orbit at an altitude of around 1,100 km, with an inclination angle of 70°. Although the ISS-b altitude was quite high for the detection of EPBs, the EPB distributions derived from the ISS-b observations from April 1978 to December 1980 (around the solar maximum) are similar to those derived from other satellite observations at lower altitudes (Watanabe & Oya 1986; Kil & Heelis 1998; McClure et al. 1998; Burke 2004; Henderson et al. 2005; Stolle et al. 2006; Su et al. 2006; Kil et al. 2009; Park et al. 2009; Gentile et al. 2011; Huang et al. 2014; Smith & Heelis 2018; Wan et al. 2018; Yizengaw & Groves 2018; Aa et al. 2019).

Fig. 2 shows the distribution of irregularities as a function of longitude and month derived from the measurements of the plasma density by ROCSAT-1 from March 1999 to June 2004 (Kil et al. 2009). ROCSAT-1 orbits were near circular at an altitude of 600 km, with an orbital inclination of 35°. Irregularities were detected by using a parameter similar to S, but the occurrence probability of irregularities was derived by smoothing the parameter for 100 data points. The occurrence of irregularities was determined when the ROCSAT-1 observations were available within ±10° dip latitudes and 20:00–00:00 local solar time (LT). These latitude and LT intervals were chosen because EPBs develop near the magnetic equator and preferentially at premidnight. The solar activity was maximum around 2001 and started to decline beginning in 2003. The occurrence rate of irregularities decreased as the solar activity declined. Irregularities occurred most frequently in the African sector (0°–30°E longitude) in most months. In the South American sector (90°–30°W longitude), irregularities occurred frequently around December solstices, but they rarely occurred around June solstices. In the Asian sector (around 150°E longitude), irregularities rarely occurred around December solstices. The recurrence of a similar pattern year after year indicates the systematic seasonal and longitudinal behavior of EPBs. The EPB distribution shown in Fig. 2 is the representative EPB climatology identified from many other observations. When we discuss the EPB climatology, the main interest is the seasonal and longitudinal pattern. Because the occurrence probability depends on the detection parameter, detection threshold, and calculation method of the probability, values found in different reports are not directly comparable.

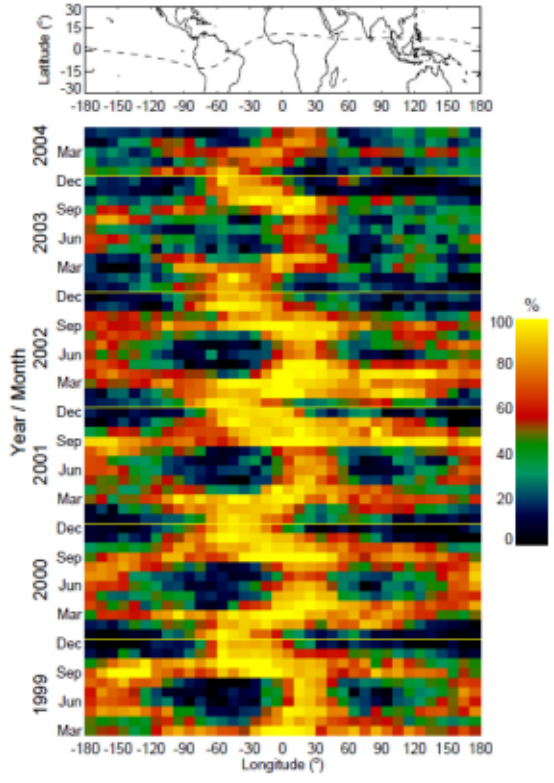

Fig. 2. EPB distribution derived from the measurements of ion density by ROCSAT-1. Adapted from Kil et al. (2009) with CC-BY. EPB, equatorial plasma bubble; ROCSAT-1, Republic of China satellite.

3. DRIVERS OF THE NIGHTTIME EQUATORIAL PLASMA BUBBLE (EPB) CLIMATOLOGY

Just after sunset, the formation of a steep vertical plasma density gradient at the bottomside of the F region, the vertical motion of the ionosphere, and the reduction of E region plasma density provide favorable conditions for the development of EPBs at the magnetic equator by the generalized Rayleigh-Taylor (GRT) instability. Two essential elements for the development of EPBs under these conditions are initial seed perturbations on the bottomside of the F region and the growth of these perturbations. The seasonal and longitudinal behavior of EPBs appear to be determined by a combination of these two factors. However, their relative significance is difficult to identify because information on both factors is not available most of the time. This is in part because observations of the atmosphere and ionosphere at the bottomside height (below an altitude of 300 km) are rare. Also, the calculation of the growth rate of the GRT instability requires simultaneous observations of many atmospheric and ionospheric parameters.

3.1 Seed Perturbations

Atmospheric gravity waves (AGWs) have long been suspected as the source of initial seed perturbations for EPBs (Whitehead 1971; Röttger 1973, 1976, 1982; Beer 1974; McClure et al. 1998; Makela et al. 2010; Tsunoda 2010;

Huang et al. 2013a; Abdu et al. 2015). AGWs derive the up and down motions of plasma along magnetic field lines by neutral-plasma collisions that result in the modulation of plasma density. The changes in the neutral composition and temperature at a given height by AGWs also affect the plasma density. When the phase velocity of AGWs matches the horizontal plasma drift velocity (spatial resonance), the density perturbations produced by AGWs persist (Whitehead 1971; Klostermeyer 1978; Huang & Kelley 2009). In addition, the electric fields generated by neutral winds accompanying AGWs can affect the ionospheric dynamics and, consequently, the generation of EPBs. The important role of AGWs in the generation of EPBs has been emphasized, but there is still no good way to trace the propagation of AGWs from lower atmosphere to the bottomside of the F region. For this reason, the presence of AGWs is inferred from the observations of wave-like modulations in the ionospheric height or plasma density (Singh et al. 1997; Kelley et al. 1981; Tsunoda & White 1981; Thampi et al. 2009; Tsunoda 2010).

The observations of the ionosphere by the 50 MHz incoherent backscatter radar at Jicamarca in Peru (12.0°S, 76.9°W) show the development of EPBs in the presence of large-scale modulations of the bottomside F region. The radar detects the backscatter echoes from thermal fluctuations of electrons, but electron density irregularities of 3-m scale produce strong echoes. The wave-like modulation of strong echoes (dark structures) in the backscatter maps in Kelley et al. (1981) represents the unstable bottomside F layer. The vertically extended and tilted backscatter plumes are the signatures of EPBs. During four consecutive days, from 19 to 22 March, the modulation of the bottomside F region was most significant on 21 March, which was also when the most intense EPBs were detected. These observations were interpreted as evidence of the role of AGWs in the generation of EPBs.

The existence of AGWs is also inferred from EPB spacing. Series of EPBs in satellite observations (Singh et al. 1997; Huang et al. 2013a) and airglow images (Takahashi et al. 2009; Makela et al. 2010) often appear to be spatially quasiperiodic. The measurements of ion density by the Communication/Navigation Outage Forecasting System satellite on two days in April 2012 are shown in Fig. 3 (Huang et al. 2013a). EPBs are indicated with yellow shading. Huang et al. (2013a) hypothesized that spatially periodic EPBs could be generated by temporal periodicity of seeding AGWs; EPBs appear to be spatially periodic, if EPBs continuously develop at the sunset terminator in the presence of AGWs. Following this hypothesis, a few tens-of-minutes periods of AGWs produce several-hundred-kilometer distances between EPBs. However, Choi et al. (2016) showed that the manner in which EPBs occur in satellite observations is not represented by waves in general, because spacing between EPBs is not represented by a specific wave. Although a series of EPBs appears to be periodic, their spatial distribution is represented by many wave components. Radar observations in Kelley et al. (1981) show the development of multiple EPBs from one side of a wave-like modulation. Because the generation of EPBs is not limited to the crest locations of a wave, the characteristic of AGWs is difficult to identify from the EPB spacing.

The wave-like modulation of the bottomside F region before the development of EPBs has been given different names: large-scale wave structure (LSWS) (Tsunoda 2010; Tsunoda et al. 2010) and bottomtype layer (Hysell et al. 2005). These phenomena can be understood in terms of AGWs, but the modulations in the ionosphere can also be produced by the Kelvin-Helmholtz instability in the presence of the shear in the zonal plasma motion (Hysell et al. 2005). Traveling ionospheric disturbances can also be the source of seed perturbations (Krall et al. 2011; Yokoyama et al. 2011a, b; Taori et al. 2015; Takahashi et al. 2018). The seeding mechanism of the bottomside F region is still an open question. The main drawback in the study of the seeding mechanism is the lack of the observations of the ionosphere

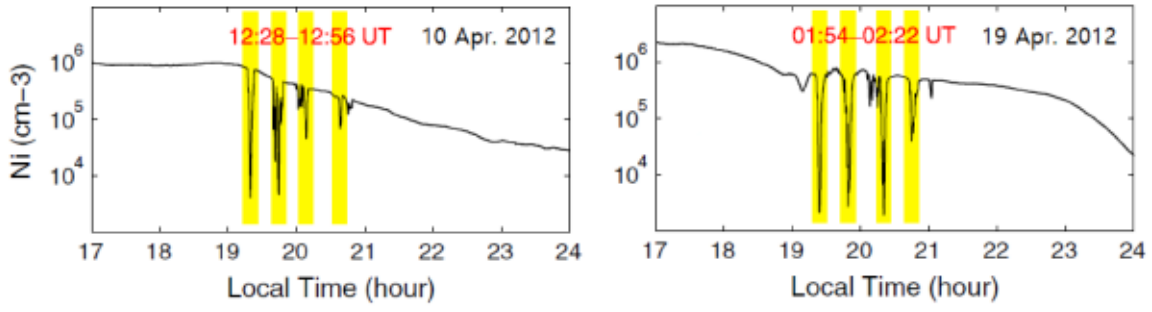

Fig. 3. Samples of quasiperiodic EPBs in C/NOFS observations. Adapted from Huang et al. (2013a) with CC-BY. EPB, equatorial plasma bubble; C/NOFS, communications/navigation outage forecasting system.

and atmosphere at the height of the bottomside F region. Therefore, the interpretation of the EPB climatology by seed perturbations is limited.

3.2 Growth Conditions

AGWs can provide seed perturbations in the bottomside of the F region, but the perturbations can grow to EPBs when they are amplified by the GRT instability. The linear growth rate of the GRT instability (γ_{GRT}) (Zalesak et al. 1982; Sultan 1996) is given as

$$\gamma_{GRT} = \frac{\Sigma_P^F}{\Sigma_P^E + \Sigma_P^F}\left(V_P - U_L^P - \frac{g_e}{\nu_{eff}^F}\right)K^F - R_T. \quad (2)$$

Σ_P^E and Σ_P^F are flux-tube integrated Pedersen conductivities in the E and F regions, respectively. V_p is the flux-tube integrated plasma velocity perpendicular to the magnetic field, which is equivalent to the zonal electric field. U_L^P is the Pedersen conductivity-weighted neutral winds in the radial direction. g_e is an effective gravitational acceleration, and ν_{eff}^F is an effective F region ion-neutral collision frequency weighted by number density along the flux tube. K^F is the F region flux tube electron content height gradient. R_T is the flux-tube integrated recombination rate. Among these parameters in the growth rate, the key factor that enables the development of EPBs after sunset is the reduction of Σ_P^E in the dark by the rapid loss of molecular ions in the E region. Because Σ_P^E is the flux-tube integrated conductivity, it is minimal when the magnetic conjugate E regions in both hemispheres are simultaneously in the dark. The simultaneity varies with season and longitude because the solar zenith angle varies with season and the magnetic declination varies with longitude. The idea that magnetic declination controls EPB activity was based on the similar seasonal and longitudinal behaviors of the sunset time at the conjugate E regions and the EPB occurrence.

Abdu et al. (1981) reported the differences in vertical plasma motions around the sunset terminator and the occurrence of EPBs at two stations in South America where the magnetic declinations were different. These differences were consistent with the difference in the simultaneity of the sunset times at the conjugate E regions. Tsunoda (1985) calculated the annual variation of sunset times at the magnetic conjugate E regions at different longitudes and investigated its correlation with the scintillation occurrence. The calculation results at some selected locations are shown in Fig. 4. Sinusoidal curves are the sunset times at the conjugate E region for four latitudinal distances (l) from the dip equator. The nodes of the curves are formed when the LTs of the sunsets at the conjugate E regions are identical. The days of the nodes vary systematically depending on the magnetic declination and the displacement of the magnetic equator from the geographic equator. For a comparison, the plots show the scintillation data from different reports. The occurrence rates of scintillations peak around the nodes. Thus, the magnetic declination is a good indicator of the global-scale scintillation (or EPB) morphology.

An important phenomenon associated with the simultaneity of the conjugate E region sunset is the uplift of the ionosphere just before the sunset. This phenomenon, often referred to as pre-reversal enhancement (PRE) or post-sunset rise (PSSR), represents a local upward plasma motion for roughly a couple of hours around 18:00 LT before the transition of the daytime upward plasma motion to nighttime downward plasma motion. The critical role of the PRE in the generation of EPBs has been demonstrated by a range of observations (Farley et al. 1970, 1986; Abdu et al. 1981, 1992, 2006; Tsunoda & White 1981; Basu et al. 1996; Fagundes et al. 1999; Fejer et al. 1999; Anderson et al. 2004; Li et al. 2008; Su et al. 2008; Smith et al. 2015). The PRE can promote the growth of EPBs by reducing the ion-neutral collision rate, producing a steep vertical gradient in the plasma density, and increasing the F region conductivity. Therefore, PRE is recognized as the single most important parameter for the generation of EPBs. Because the generation of the PRE is determined by various E and F region parameters, including magnetic declination, and E and F region conductivities, and F region dynamo, PRE is a comprehensive parameter that represents the growth condition of EPBs.

Fig. 5 presents the maps of the (middle) EPB occurrence probability and (bottom) PRE as a function of longitude and month (Kil et al. 2009). The dashed line in the top panel indicates the magnetic equator. The EPB occurrence probability was derived by using the ROCSAT-1 data around the solar maximum (1999–2002) for Kp ≤ 3^+. PRE was calculated by using the data within ±5° dip latitudes at 17:30–19:30 LT. The distributions of EPB and PRE show good agreement. On average, EPBs occur frequently at all longitudes during equinoxes. The annual variation of the EPB occurrence probability is pronounced in the Indian and American-Atlantic sectors. PRE shows a similar behavior. Therefore, a significant portion of the seasonal and longitudinal behavior of EPBs is explained by the PRE.

The maps in Fig. 5 provide an opportunity to examine the role of the magnetic declination in EPB and PRE generation. Their annual behaviors at 30°–60°W longitude (negative magnetic declination) show higher EPB occurrence

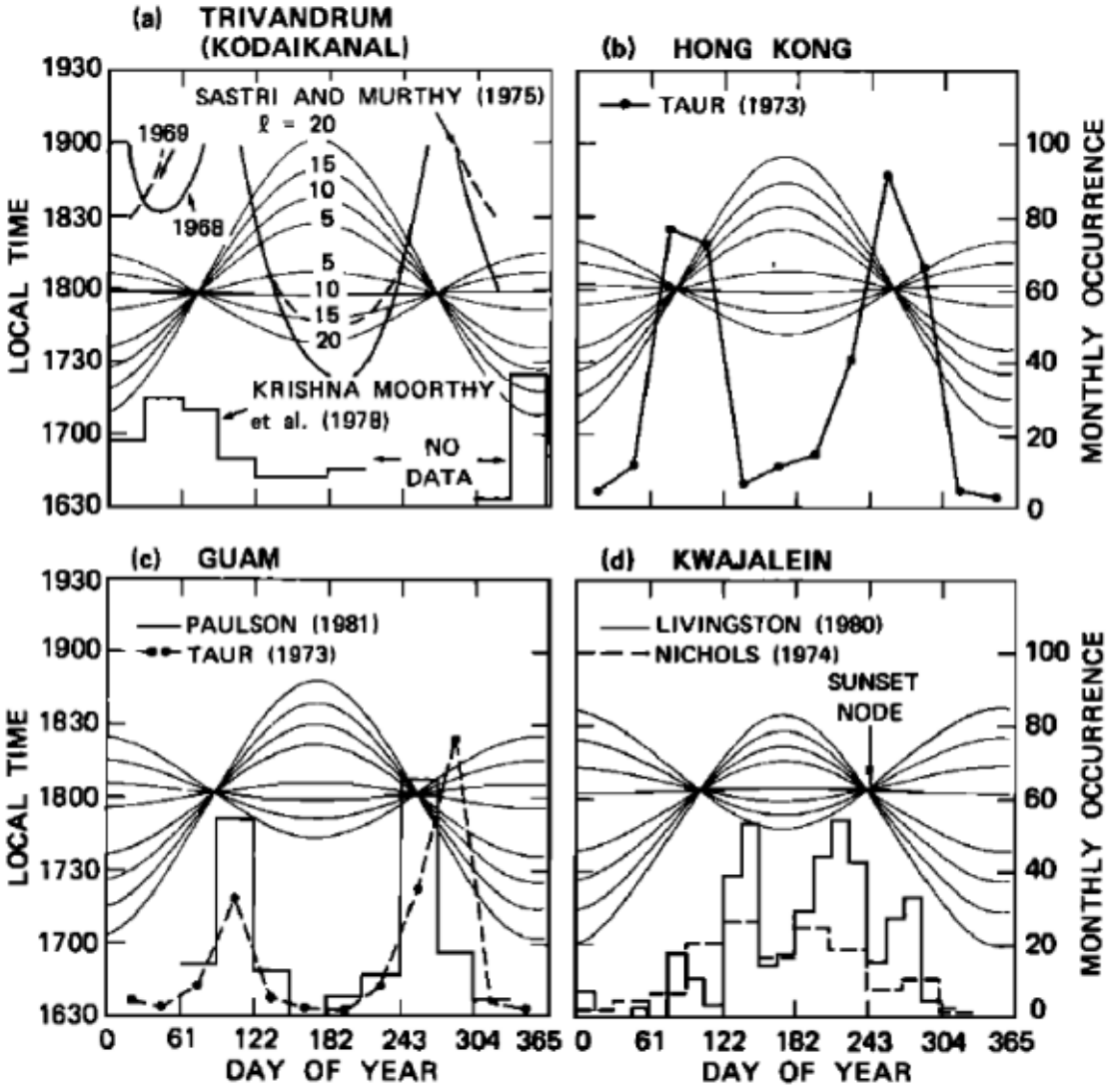

Fig. 4. Comparisons of conjugate E region sunset times for different dip latitudes (sinusoidal curves) and scintillation occurrence rates at different stations. Adapted from Tsunoda (1985) with permission of John Wiley & Son. The *l* values indicate the latitudinal distance from the dip equator.

probability and greater PRE value around the December solstice than around the June solstice. This observation is consistent with the idea that magnetic declination controls EPB and PRE. However, their annual behaviors around 90°W longitude (positive magnetic declination) are not explained by the magnetic declination. The annual distributions of EPB and PRE vary largely in 0°–120°E longitude, although the magnetic declination does not change much in this longitude region. These observations are not explained by the E region conductivity or magnetic declination. In addition to the E region conductivity, many other factors, including the F region plasma distribution, neutral winds, and background electric and magnetic fields, affect the PRE and growth rate of the GRT. The combined effect of these factors are not yet fully understood.

4. DAYTIME EQUATORIAL PLASMA BUBBLEs (EPBs)

EPBs are nighttime phenomena because photoionization after sunrise rapidly fills plasma depletions. Because of the rapid decay of EPBs in sunlight, little attention has been paid to the evolution of EPBs on the dayside. However, recent studies of daytime irregularities in the equatorial region show the persistence of EPBs even after sunrise (Huang et al. 2013b; Kil et al. 2019, 2020). The daytime irregularities noted in these studies were detected in regions where EPBs were detected on the previous night. Therefore, daytime irregularities in the equatorial region are interpreted as fossils of nighttime EPBs.

Because ROCSAT-1 had low-inclination orbits, it revisited

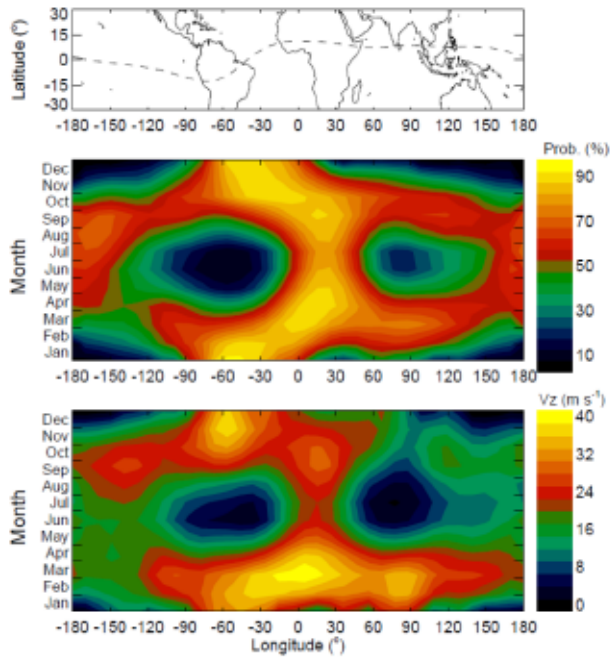

Fig. 5. Comparison of the distributions of (middle) EPB occurrence probability and (bottom) PRE magnitude. Adapted from Kil et al. (2009) with CC-BY. In the top panel, the dashed line indicates the magnetic equator. EPB, equatorial plasma bubble; PRE, pre-reversal enhancement.

the same longitude region several times a day. These observations enable tracing of the evolution of nighttime EPBs into the dayside. In the ROCSAT-1 observations in Fig. 6 (Kil et al. 2019), small amplitude irregularities are detected on the dayside along the satellite orbits (2, 3, and 4). Irregularity locations are indicated by red in the satellite orbits. The observations on the previous nights (orbit 1) reveal the development of strong EPBs at postmidnight at the longitudes where daytime irregularities were detected. The connection of daytime irregularities to nighttime EPBs is further supported by the similar seasonal and longitudinal behavior of the nighttime and daytime irregularities (Kil et al. 2020).

A distinguishing characteristic of daytime irregularities is their latitudinal distribution. Nighttime irregularities are concentrated near the magnetic equator, but the concentration of daytime irregularities moves from the magnetic equator to high latitudes with time (Kil et al. 2019). This behavior is attributed to the vertical motion of the ionosphere on the dayside; the vertical motion induces the transport of the fossil EPBs at the magnetic equator to higher latitudes, as if equatorial plasma is latitudinally redistributed by the fountain effect. The role of the fountain effect in the evolution of daytime irregularities is further manifested by the longitudinal distribution of daytime irregularities. Fig. 7 shows the longitudinal distributions of daytime (10:00–14:00 LT) irregularities and plasma density for two seasons derived from the ROCSAT-1 data in 1999–2004: (a, b) June–September, (c, d) November–February (Kil et al. 2020). The white lines in the plots are the vertical ion velocity. June–September is the period during which longitudinal wave number 4 pattern develops in the plasma density and vertical plasma motion by nonmigrating zonal wave number 3 tide. The wave number 4 pattern is identified from the daytime irregularity distribution and from the plasma density in June–September. The morphologies of the daytime irregularities and plasma density are also similar in November–February. Their seasonal and longitudinal behaviors are consistent with vertical plasma motion. In addition to the latitudinal redistribution of fossil EPBs, the fountain effect can also affect the lifetime of fossil EPBs. Because the photoionization rate decreases with increasing altitude, fossil EPBs can survive longer at higher altitudes. The latitudinal redistribution also influences the fossil EPB lifetime because the variation of the solar zenith angle affects the photoionization rate.

5. CONCLUDING REMARKS

The importance of the uplift of the F region by the PRE for the generation of EPBs was demonstrated by many observations and numerical simulations. A significant portion of the EPB occurrence climatology and the day-to-day variability of EPB activity is explained in terms of the PRE. The high chance of EPB detection under a strong PRE regardless of the presence of AGWs may indicate the prevalence of seed perturbations. In that case, the role of seed perturbation is minor compared with the role of the PRE in the generation of EPBs. Seed perturbations may play a role when the growth condition of EPBs is marginal. The role of AGWs is often confined to the source of seed perturbations, but AGWs can be understood as a component of the growth condition of EPBs because AGW winds would affect the dynamo process in the E and F regions.

The characteristics of irregularities around June solstices and during solar minimum are different from those during other periods. Around June solstices and during solar minimum, small amplitude irregularities frequently occur around midnight. One of the reasons for the different behavior of the irregularities during these periods can be attributed to the different behavior of the PRE. The phenomenon of the "midnight temperature maximum" in the thermosphere has also been suggested to explain the generation of irregularities around midnight (Fang et al. 2016). In addition, the generation of equatorial irregularities by medium-scale traveling disturbances (MSTIDs) is worth investigating. Because MSTIDs preferentially develop

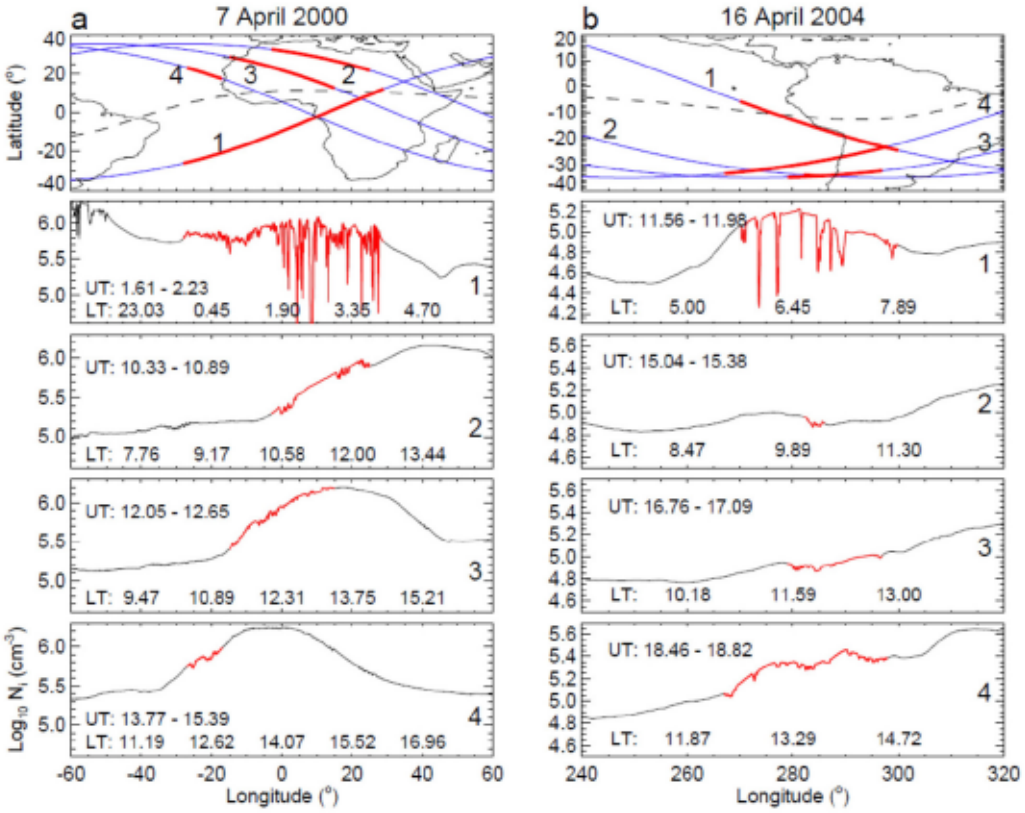

Fig. 6. Tracing of the history of daytime irregularities shown in the ROCSAT-1 observations. Adapted from Kil et al. (2019) with CC-BY. In the ROCSAT-1 orbits and density data (orbits 2–4), the locations of daytime irregularities are indicated in red. Orbit 1 for both days is the orbit on the previous night. ROCSAT-1, Republic of China satellite.

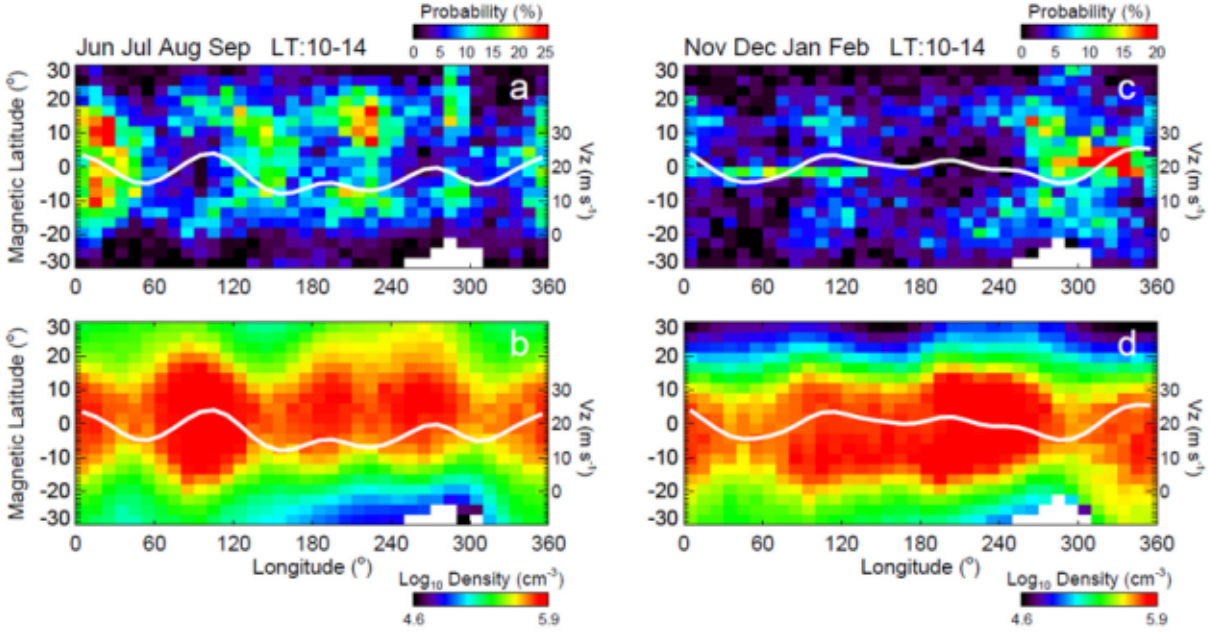

Fig. 7. Comparison of the distributions of daytime irregularities and plasma density in two seasons. The white curves are the vertical ion velocities. The results were derived from the ROCSAT-1 data at 10:00–14:00 LT in March 1999–June 2004. Adapted from Kil et al. (2020) with CC-BY. ROCSAT-1, Republic of China satellite; LT, local solar time.

near midnight and around June solstices and during solar minimum, some of the irregularities during these periods may be associated with MSTIDs.

The morphology of daytime irregularities indicates the latitudinal redistribution of fossil EPBs by the fountain effect. In addition to the latitudinal redistribution, the fountain effect affects the lifetime of fossil EPBs by transporting them to higher altitudes and higher latitudes. EPBs can survive longer at higher altitudes and at higher latitudes because the production rate decreases under these conditions. Numerical simulations are desired for the evaluation of this hypothesis.

ACKNOWLEDGMENTS

This work was supported by National Science Foundation (no. AGS2029840), Air Force Multi-University Research Initiative (no. FA9559-16-1-0364), and Air Force Asian Office of Aerospace Research and Development (no. FA2386-21-1-4034) in the United States.

ORCID

Hyosub Kil https://orcid.org/0000-0001-8288-6236

REFERENCES

Aa E, Zou S, Liu S, Statistical analysis of equatorial plasma irregularities retrieved from Swarm 2013–2019 observations, J. Geophys. Res. Space Phys. 125(4), e2019JA027022 (2020) https://doi.org/10.1029/2019ja027022

Aarons J, Global morphology of ionospheric scintillations, Proceedings of the IEEE, 70, 360-378 (1982). https://doi.org/10.1109/PROC.1982.12314

Aarons J, The longitudinal morphology of equatorial F layer irregularities relevant to their occurrence, Space Sci. Rev. 63, 209-243 (1993). https://doi.org/10.1007/BF00750769

Abdu MA, Batista IS, Sobral JHA, A new aspect of magnetic declination control of equatorial spread F and F-region dynamo, J. Geophys. Res. 97, 14897-14904 (1992). https://doi.org/10.1029/92JA00826

Abdu MA, Batista PP, Batista IS, Brum CGM, Carrasco AJ, et al., Planetary wave oscillations in mesospheric winds, equatorial evening prereversal electric field and spread F, Geophys. Res. Lett. 33, L07107 (2006). https://doi.org/10.1029/2005GL024837

Abdu MA, Bittencourt JA, Batista IS, Magnetic declination control of the equatorial F-region dynamo electric field development and spread F, J. Geophys. Res. 86, 11443-11446 (1981). https://doi.org/10.1029/JA086iA13p11443

Abdu MA, de Souza JR, Kherani EA, Batista IS, MacDougall JW, et al., Wave structure and polarization electric field development in the bottomside F layer leading to postsunset equatorial spread F, J. Geophys. Res. Space Phys. 120, 6930-6940 (2015). https://doi.org/10.1002/2015JA021235

Anderson DN, Reinisch BW, Valladares C, Chau J, Veliz O, Forecasting the occurrence of ionospheric scintillation activity in the equatorial ionosphere on a day-to-day basis, J. Atmos. Sol. Terr. Phys. 66, 1567-1572 (2004). https://doi.org/10.1016/j.jastp.2004.07.010

Basu S, Basu S, Equatorial scintillations: a review, J. Atmos. Terr. Phys. 43, 473-489 (1981). https://doi.org/10.1016/0021-9169(81)90110-0

Basu S, Basu S, Khan, BK, Model of equatorial scintillations from in-situ measurements, Radio Sci. 11, 821-832 (1976). https://doi.org/10.1029?RS011i010p00821

Basu S, Kudeki E, Basu Su, Valladares CE, Weber EJ, et al., Scintillation, plasma drifts, and neutral winds in the equatorial ionosphere after sunset, J. Geophys. Res. 101, 26795-26809 (1996). https://doi.org/10.1029/96JA00760

Beer T, Atmospheric Waves (John Wiley & Son, New York, NY, 1974).

Burke WJ, Longitudinal variability of equatorial plasma bubbles observed by DMSP and ROCSAT-1, J. Geophys. Res. 109, A12301 (2004). https://doi.org/10.1029/2004ja010583

Burke WJ, Donatelli DE, Sagalyn RC, Kelley MC, Low density regions observed at high altitudes and their connection with equatorial spread F, Planet. Space Sci. 27, 593-601 (1979). https://doi.org/10.1016/0032-0633(79)90157-0

Choi JM, Kil H, Kwak YS, Park J, Lee WK, et al., Periodicity in the occurrence of equatorial plasma bubbles derived from the C/NOFS observations in 2008–2012, J. Geophys. Res. Space Phys. 121 (2016). https://doi.org/10.1002/2016JA023528

Fagundes PR, Sahai Y, Batista IS, Abdu MA, Bittencourt JA, et al., Observations of day-to-day variability in precursor signatures to equatorial F-region plasma depletions, Ann. Geophys. 17, 1053-1063 (1999). https://doi.org/10.1007/s00585-999-1053-x

Fang TW, Akmaev RA, Stoneback RA, Fuller-Rowell T, Wang H, et al., Impact of midnight thermosphere dynamics on the equatorial ionospheric vertical drifts, J. Geophys. Res. Space Phys. 121, 4858-4868 (2016). https://doi.org/10.1002/2015JA022282

Farley DT, Balsley B, Woodman RF, McClure JP, Equatorial spread F: implications of VHF radar observations, J. Geophys. Res. 75, 7199-7216 (1970). https://doi.org/10.1029/JA075i034p07199

Farley DT, Bonelli E, Fejer BG, Larsen MF, The prereversal enhancement of the zonal electric field in the equatorial

ionosphere, J. Geophys. Res. 91, 13723-13728 (1986). https://doi.org/10.1029/JA091iA12p13723

Fejer BG, Scherliess L, de Paula ER, Effects of the vertical plasma drift velocity on the generation and evolution of equatorial spread F, J. Geophys. Res. 104, 19859-19869 (1999). https://doi.org/10.1029/1999JA900271

Gentile LC, Burke WJ, Roddy PA, Retterer JM, Tsunoda RT, Climatology of plasma density depletions observed by DMSP in the dawn sector, J. Geophys. Res. Space Phys. 116 (2011). https://doi.org/10.1029/2010ja016176

Hanson WB, Sanatani S, Relationship between Fe^{+} ions and equatorial spread F, J. Geophys. Res. 76, 7761-7768 (1971). https://doi.org/10.1029/JA076i031p07761

Henderson SB, Swenson CM, Christensen AB, Paxton LJ, Morphology of the equatorial anomaly and equatorial plasma bubbles using image subspace analysis of Global Ultraviolet Imager data, J. Geophys. Res. 110, A11306 (2005). https://doi.org/10.1029/2005JA011080

Huang CS, de La Beaujardiere O, Roddy PA, Hunton DE, Ballenthin JO, et al., Large-scale quasiperiodic plasma bubbles: C/NOFS observations and causal mechanism, J. Geophys. Res. Space Phys. 118, 3602-3612 (2013a). https://doi.org/10.1002/jgra.50338

Huang CS, de La Beaujardiere O, Roddy PA, Hunton DE, Ballenthin JO, et al., Long-lasting daytime equatorial plasma bubbles observed by the C/NOFS satellite, J. Geophys. Res. Space Phys. 118, 2398-2408 (2013b). https://doi.org/10.1002/jgra.50252

Huang CS, Kelley MC, Nonlinear evolution of equatorial spread F: 1. on the role of plasma instabilities and spatial resonance associated with gravity wave seeding, J. Geophys. Res. 101, 283-292 (2009). https://doi.org/10.1029/95JA02211

Huang CS, La Beaujardiere O, Roddy PA, Hunton DE, Liu JY, et al., Occurrence probability and amplitude of equatorial ionospheric irregularities associated with plasma bubbles during low and moderate solar activities (2008–2012), J. Geophys. Res. Space Phys. 119, 1186-1199 (2014). https://doi.org/10.1002/2013JA019212

Hysell DL, Kudeki E, Chau JL, Possible ionospheric preconditioning by shear flow leading to equatorial spread F, Ann. Geophys. 23, 2647-2655 (2005). https://doi.org/10.5194/angeo-23-2647-2005

Kelley MC, Larsen MF, LaHoz C, McClure JP, Gravity wave initiation of equatorial spread F: a case study, J. Geophys. Res. 86, 9087-9100 (1981) https://doi.org/10.1029/JA086iA11p09087

Kil H, The morphology of equatorial plasma bubbles: a review, J. Astron. Space Sci. 32, 13-19 (2015). https://doi.org/10.5140/JASS.2015.32.1.13

Kil H, Heelis RA, Global distribution of density irregularities in the equatorial ionosphere, J. Geophys. Res. Space Phys. 103, 407-417 (1998). https://doi.org/10.1029/97ja02698

Kil H, Lee WK, Paxton LJ, Origin and distribution of daytime electron density irregularities in the low-latitude F region, J. Geophys. Res. Space Phys. 125, e2020JA028343 (2020). https://doi.org/10.1029/2020JA028343

Kil H, Paxton LJ, Lee WK, Jee G. Daytime evolution of equatorial plasma bubbles observed by the first Republic of China satellite, Geophys. Res. Lett. 46, 5021-5027 (2019). https://doi.org/10.1029/2019gl082903

Kil H, Paxton LJ, Oh SJ, Global bubble distribution seen from ROCSAT-1 and its association with the evening prereversal enhancement, J. Geophys. Res. Space Phys. 114, A06307 (2009). https://doi.org/10.1029/2008ja013672

Klostermeyer J, Nonlinear investigation of the spatial resonance effect in the nighttime equatorial F region, J. Geophys. Res. 83, 3753-3760 (1978). https://doi.org10.1029/JA083iA08p03753

Krall J, Huba JD, Ossakow SL, Joyce G, Makela JJ, et al., Modeling of equatorial plasma bubbles triggered by non-equatorial traveling ionospheric disturbances, Geophys. Res. Letts 38, L08103 (2011). https://doi.org/10.1029/2011GL046890

Li G, Ning B, Liu L, Ren Z, Lei J, et al., The correlation of longitudinal/seasonal variations of evening equatorial pre-reversal drift and of plasma bubbles, Ann. Geophys. 25, 2571-2578 (2008). https://doi.org/10.5194/angeo-25-2571-2007

Makela JJ, Vadas SL, Muryanto R, Duly T, Crowley G, Periodic spacing between consecutive equatorial plasma bubbles, Geophys. Res. Lett. 37, L14103 (2010). https://doi.org/10.1029/2010GL043968.

Maruyama T, Matuura N, Longitudinal variability of annual changes in activity of equatorial spread F and plasma bubbles, J. Geophys. Res. 89, 10903-10912 (1984). https://doi.org/10.1029/ja089ia12p10903

McClure JP, Singh S, Bamgboye DK, Johnson FS, Kil H, Occurrence of equatorial F region irregularities: evidence for tropospheric seeding, J. Geophys. Res. Space Phys. 103, 29119-29135 (1998). https://doi.org/10.1029/98ja02749

Park J, Lühr H, Stolle C, Rother M, Min KW, et al., The characteristics of field-aligned currents associated with equatorial plasma bubbles as observed by the CHAMP satellite, Ann. Geo. 27, 2785-2697 (2009). https://doi.org/10.5194/angeo-27-2685-2009

Röttger J, Wave-like structures of large-scale equatorial spread-F irregularities, J. Atmos. Terr. Phys. 36, 1195-1196 (1973). https://http://dx.doi.org/10.1016/0021-9169(73)90016-0doi.org/10.1016/0021-9169(73)90016-0

Röttger J, The macro-scale structure of equatorial spread-F irregularities, J. Atmos. Terr. Phys. 38, 97-101 (1976). https://doi.org/10.1016/0021-9169(76)90200-2

Röttger J, Equatorial spread F by electric fields and atmospheric

gravity waves generated by thunderstorms, J. Atmos. Terr. Phys. 43, 453-462 (1982). https://doi.org/10.1016/0021-9169(81)90108-2

Singh S, Johnson FS, Power RA, Gravity wave seeding of equatorial plasma bubbles, J. Geophys. Res. 102, 7399-7410 (1997). https://doi.org/0148-0227/97/96JA03998509.00

Smith JM, Heelis RA, The plasma environment associated with equatorial ionospheric irregularities. J. Geophy. Res. Space Phys. 123, 1583-1592 (2018). https://doi.org/10.1002/2017JA024933

Smith JM, Rodrigues FS, de Paula ER, Radar and satellite investigations of equatorial evening vertical drifts and spread F, Annales Geophysicae, 33, 1403-1412 (2015). https://doi.org/10.5194/angeo-33-1403-2015

Stolle C, Lühr H, Rother M, Balasis G, Magnetic signatures of equatorial spread F as observed by the CHAMP satellite, J. Geophys. Res. 111, A02304 (2006). https://doi.org/10.1029/2005ja011184

Su SY, Chao CK, Liu CH, On monthly/seasonal/longitudinal variations of equatorial irregularity occurrences and their relationship with the post-sunset vertical drift velocities, J. Geophys. Res, 113, A05307 (2008). https://doi.org/10.1029/2007JA012809

Su SY, Liu CH, Ho HH, Chao CK, Distribution characteristics of topside ionospheric density irregularities: equatorial versus midlatitude regions, J. Geophys. Res. 111, A06305 (2006). https://doi.org/10.1029/2005ja011330

Sultan PJ, Linear theory and modeling of the Rayleigh-Taylor instability leading to the occurrence of equatorial spread F, J. Geophys. Res. 101, 26875-26891 (1996). http://doi.org/10.1029/96JA00682

Takahashi H, Tayler MJ, Pautet PD, Medeiros AF, Gobbi D et al., Simultaneous observation of ionospheric plasma bubbles and mesospheric gravity waves during the SpreadFEx Campaign, Ann. Geophys. 27, 1477-1487 (2009). https://doi.org/10.5194/angeo-27-1477-2009

Takahashi H, Wrasse CM, Figueiredo CAOB, Barros D, Abdu MA, et al., Equatorial plasma bubble seeding by MSTIDs in the ionosphere, Prog. Earth Planet. Sci. 5, 32 (2018). https://doi.org/10.1186/s40645-018-0189-2

Taori A, Parihar N, Ghodpage R, Dashora N, Sripathi S, et al., Probing the possible trigger mechanisms of an equatorial plasma bubble event based on multistation optical data, J. Geophys. Res. Space Phys. 120 (2015). https://doi.org/10.1002/2015JA021541

Thampi SV, Yamamoto M, Tsunoda RT, Otsuka Y, Tsugawa TJ, et al., First observations of large-scale wave structure and equatorial spread F using CERTO radio beacon on the C/NOFS satellite, Geophys. Res. Lett. 36, L18111 (2009). https://doi.org/10.1029/ 2009GL039887

Tsunoda RT, Control of the seasonal and longitudinal occurrence of equatorial scintillations by the longitudinal gradient in integrated E region Pedersen conductivity, J. Geophys. Res. Space Phys. 90, 447-456 (1985). https://doi.org/10.1029/ja090ia01p00447

Tsunoda RT, On seeding equatorial spread F during solstices, Geophys. Res. Lett. 37, L05102 (2010). https://doi.org/10.1029/2010GL042576

Tsunoda RT, Bubenik DM, Thampi SV, Yamamoto M, On large-scale wave structure and equatorial spread F without a post-sunset rise of the F layer, Geophys. Res. Lett. 37, L07105 (2010). https://doi.org/10.1029/2009GL042357

Tsunoda RT, White BR, On the generation and growth of equatorial backscatter plumes 1. Wave structure in the bottomside F layer, J. Geophys. Res. 86, 3610-3616 (1981) https://doi.org/10.1029/JA086iA05p03610

Wan X, Xiong C, Rodriguez-Zuluaga J, Kervalishvili GN, Stolle C, et al., Climatology of the occurrence rate and amplitudes of local time distinguished equatorial plasma depletions observed by Swarm satellite, J. Geophys. Res. Space Phys. 123, 3014-3026 (2018). https://doi.org/10.1002/2017JA025072

Watanabe S, Oya H, Occurrence characteristics of low latitude ionosphere irregularities observed by impedance probe on board the Hinotori satellite. J. Geomagn. Geoelectr. 38, 125-149 (1986). https://doi.org/10.5636/jgg.38.125

Whitehead JD, Ionization disturbances caused by gravity waves in the presence of an electrostatic field and background wind, J. Geophys. Res. 76, 238-241 (1971). https://doi.org/10.1029/JA076i001p00238

Yizengaw E, Groves KM, Longitudinal and seasonal variability of equatorial ionospheric irregularities and electrodynamics. Space Weather, 16, 946-968 (2018). https://doi.org/10.1029/2018SW001980

Yokoyama T, Pfaff RF, Roddy PA, Yamamoto M, Otsuka Y, On postmidnight low-latitude ionospheric irregularities during solar minimum: 2. C/NOFS observations and comparisons with the Equatorial Atmosphere Radar, J. Geophys. Res. 116, A11326 (2011b). https://doi.org/10.1029/2011JA016798

Yokoyama T, Yamamoto M, Otsuka Y, Nishioka M, Tsugawa T, et al., On postmidnight low-latitude ionospheric irregularities during solar minimum: 1. Equatorial Atmosphere Radar and GPS-TEC observations in Indonesia, J. Geophys. Res. 116, A11325 (2011a). https://doi.org/10.1029/2011JA016797

Zalesak ST, Ossakow SL, Chaturvedi PK, Nonlinear equatorial spread F: the effect of neutral winds and background Pedersen conductivity, J. Geophys. Res. 87, 151-166 (1982). http://doi.org/10.1029/JA087iA01p00151